

Physical Limits on Raman Scattering: The Critical Role of Pump and Signal Co-design

Alessio Amaolo,¹ Pengning Chao,² Thomas J. Maldonado,³ Sean Molesky,⁴ and Alejandro W. Rodriguez³

¹*Department of Chemistry, Princeton University, Princeton, New Jersey 08544, USA**

²*Department of Mathematics, Massachusetts Institute of Technology, Cambridge, Massachusetts 02139, USA*

³*Department of Electrical and Computer Engineering,
Princeton University, Princeton, New Jersey 08544, USA*

⁴*Department of Engineering Physics, Polytechnique Montréal, Montréal, Québec H3T 1J4, Canada*

(Dated: March 7, 2024)

We present a rigorous method for deriving limits on Raman scattering in structured media. We exploit this framework to constrain the maximum Raman signal resulting from a planewave incident on two experimentally relevant systems, consisting of either a single Raman molecule in the vicinity of a structured medium or a designable Raman medium (a distribution of Raman molecules). Results pertaining to metallic and dielectric structures illustrate the efficacy of structural optimization and the importance of accounting and co-designing for the nonlinear interplay between pump and signal fields. In particular, we show that treating the pump-focusing and signal-extraction processes separately, as has been done in prior works, leads to highly unrealistic predictions of achievable enhancements. The formulation could readily find applications in guiding further improvements on surface-enhanced Raman scattering (SERS) sensitivity and Raman-assisted lasing.

Introduction.— Raman scattering plays an important role in the development of spectroscopic methods [1] and lasers [2]. While these processes are generally weak, Raman signals can be enhanced by nanostructuring [3], for example by focusing the source field or via the creation of optical resonances at the Raman frequency (or both) [4]. Recent attempts to assess the limitations of structuring for enhancing Raman scattering [5] have relied on linearized analyses that treat design constraints at the pump and signal frequencies independently. In this article, we present a quadratic optimization scheme to compute limits on Raman scattering that captures the inherent nonlinearity of this process and thus fully accounts for trade-offs in co-designing for the incident and Raman-scattered fields. We consider two experimentally relevant configurations, depicted in Fig. 1: (a) light incident on a Raman scatterer (a molecule) in the vicinity of a structured medium [4, 6], and (b) a designable Raman medium (a distribution of molecules) [7]. In the case of a *Raman molecule* surrounded by a circular antenna, bounds on maximum achievable signal enhancement are shown to follow trends and values seen in optimized geometries. Conversely, limits that optimize focusing and scattering sub-problems independently of one another overestimate achievable performance by one to two orders of magnitude, demonstrating that modelling the fully coupled Raman problem is crucial. Compared to prior limits which also decouple and further relax this problem [5], the largest possible Raman signals are shown to be more than four orders of magnitude smaller. In the case of a *Raman medium*, previously unexplored, results reveal achievable performance coming within factors of unity of the bound when the pump and signal frequencies are close.

The nascent ability to exploit convex optimization

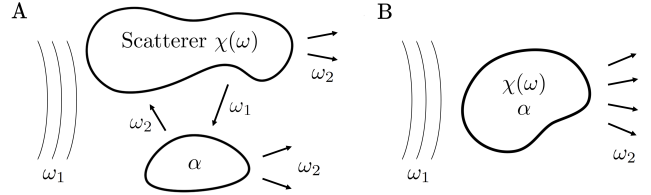


FIG. 1. Schematic of the two configurations under consideration. (A) An electromagnetic wave is incident on an arbitrarily structured medium of susceptibility $\chi(\omega)$ in the vicinity of a known Raman-active region α . (B) An electromagnetic wave is incident on a structured scatterer of susceptibility $\chi(\omega)$ and Raman polarizability α . In either case, we aim to maximize the Raman signal at ω_2 .

methods for deriving wave limits mirrors related advances in the area of structural optimization or “inverse design” [8–12]. In combination with structural optimization—an NP-hard problem that forbids efficient guarantees of optimal solutions—bounds offer a general-purpose (both geometry and mechanism agnostic) means of determining possible performance gaps. While originally confined to linear electromagnetic settings, with one recent exception [13], the present work demonstrates that quadratic optimization methods may be successfully adapted to study nonlinear wave problems, with potential applications to Raman lasers [14], frequency combs [15], and Raman amplification [16].

Formulation.— To first order in the Raman response [1], within the rotating-wave approximation [17], a source “pump” field $\mathbf{E}_1(\mathbf{r}, \omega_1)$ oscillating at frequency ω_1 incident on a Raman-active medium of polarizability $\alpha(\mathbf{r})$ generates a bound current $\mathbf{J}_2 \equiv -i\omega_2\alpha\mathbf{E}_1$ oscillating at the Raman “signal” frequency ω_2 . Maxwell’s equations (ignoring down-conversion) thus take the form

$$\mathbb{M}_1 \mathbf{E}_1(\mathbf{r}, \omega_1) = i\omega_1 \mathbf{J}_{\text{vac}}(\mathbf{r}, \omega_1) \quad (1a)$$

$$\mathbb{M}_2 \mathbf{E}_2(\mathbf{r}, \omega_2) = i\omega_2 \mathbf{J}_2(\mathbf{r}, \omega_2) = \omega_2^2 \alpha(\mathbf{r}) \mathbf{E}_1, \quad (1b)$$

where $\mathbb{M}_j = \nabla \times \nabla \times -k_j^2 \mathbb{V}(\mathbf{r}, \omega_j)$ for $j = \{1, 2\}$ are the linear Maxwell's equations for the pump and signal wavelengths, \mathbf{E}_1 is the field sourced by the initial current \mathbf{J}_{vac} , \mathbf{E}_2 is the scattered Raman field, $k_j = \omega_j/c$, $\mathbb{V}(\mathbf{r}, \omega_j)$ is the permittivity profile at ω_j , $\epsilon_0 = 1$, and we set the permeability $\mu = 1$. These equations are nonlinearly coupled in two important ways. First, the field determined by (1a) acts as a source in (1b). Second, the spatial profile of the permittivity is the same at both frequencies.

A key figure of merit in determining possible Raman enhancement from structuring is the scattered power at the Raman frequency,

$$\begin{aligned} \max_{\mathbb{P}(\mathbf{r})} \quad & -\frac{1}{2} \text{Re} \int \mathbf{J}_2^* \cdot \mathbf{E}_2 - \frac{\omega_2}{2} \int \mathbf{E}_2^* \text{Im} \mathbb{V} \mathbf{E}_2 \\ \text{s.t.} \quad & \mathbb{M}_1 \mathbf{E}_1 = i\omega_1 \mathbf{J}_{\text{vac}} \\ & \mathbb{M}_2 \mathbf{E}_2 = \omega_2^2 \alpha(\mathbf{r}) \mathbf{E}_1 \\ & \mathbb{V}(\mathbf{r}, \omega_j) = (1 + \chi(\omega_j)) \mathbb{P}(\mathbf{r}) \end{aligned} \quad (2)$$

where $\chi(\omega_j)$ is the material susceptibility at frequency ω_j and $\mathbb{P}(\mathbf{r})$ encodes the spatial susceptibility profile of the structured medium, and thus couples the two scattering problems. In (2), the first term and second term of the objective function correspond to extracted and absorbed power, respectively. If the design material is itself Raman-active, we simply take $\alpha(\mathbf{r}) = \alpha \mathbb{P}(\mathbf{r})$ for a constant polarizability tensor α . Intuitively, this quantity is often understood and optimized by relaxing the problem into two separate linear scattering processes. First, a field-focusing scheme in which the amplitude of the Raman source, proportional to the induced polarization $\alpha(\mathbf{r}) \mathbf{E}_1$ from the incident source, can be maximized:

$$\begin{aligned} \max_{\mathbb{V}(\mathbf{r}, \omega_1)} \quad & \int \bar{\mathbf{E}}_1^* \alpha(\mathbf{r})^\dagger \cdot \alpha(\mathbf{r}) \bar{\mathbf{E}}_1 \\ \text{s.t.} \quad & \mathbb{M}_1 \bar{\mathbf{E}}_1 = i\omega_1 \mathbf{J}_{\text{vac}}. \end{aligned} \quad (3)$$

Second, the scattered power at the Raman signal may be separately enhanced by solving

$$\begin{aligned} \max_{\mathbb{V}(\mathbf{r}, \omega_2)} \quad & -\frac{1}{2} \text{Re} \int (\bar{\mathbf{J}}_2)^* \cdot \mathbf{E}_2 - \frac{\omega_2}{2} \int \mathbf{E}_2^* \text{Im} \mathbb{V} \mathbf{E}_2 \\ \text{s.t.} \quad & \mathbb{M}_2 \mathbf{E}_2 = i\omega_2 \bar{\mathbf{J}}_2, \end{aligned} \quad (4)$$

where the amplitude of the Raman current source $\bar{\mathbf{J}}_2 = -i\omega_2 \alpha(\mathbf{r}) \mathbf{E}_1$ is obtained upon solving the field-focusing optimization problem. Note that such a relaxation requires prior knowledge of $\alpha(\mathbf{r})$ and therefore cannot be used to bound problems where the design material is Raman-active. While solving (3) and (4) separately offers conceptual and computational simplicity, leveraged

by existing works [5] to bound extracted power, the explicit lack of a unique structure, $\mathbb{V}(\mathbf{r}, \omega_j) = \chi(\omega_j) \mathbb{P}(\mathbf{r})$ for all $j \in \{1, 2\}$, means that solutions can overestimate possible enhancements. The scattering processes of (3) and (4) are not related by reciprocity, meaning the different structural considerations required at each wavelength would suggest higher performance than actually possible if treating these two processes separately. Maintaining the full coupling and nonlinear interplay between pump and signal fields, as achieved in this work, is therefore critically important for assessing co-design trade-offs.

We first consider the case of a *Raman molecule*, illustrated schematically in Fig. 1(A), taking $\alpha(\mathbf{r}) \rightarrow \alpha \mathbb{P}_r(\mathbf{r})$ with α a constant polarizability tensor and $\mathbb{P}_r(\mathbf{r})$ an operator that projects fields onto some prescribed (fixed) Raman scatterer: for a single molecule, $\mathbb{P}_r(\mathbf{r}) = \delta(\mathbf{r} - \mathbf{r}')$. We seek to maximize objectives of the fields with respect to the permittivity distribution of an adjacent linear structure $\mathbb{V}(\mathbf{r}, \omega_j)$. Defining \mathbb{G}_j as the operator form of the vacuum Green's function, $(\nabla \times \nabla \times - k_j^2) \mathbb{G}_j = k_j^2 \mathbb{I}$, we decompose \mathbf{E}_1 into its incident and scattered components: $\mathbf{E}_1 = \mathbf{E}_{i,1} + \mathbf{E}_{s,1} = \mathbf{E}_{i,1} + \frac{iZ}{k_1} \mathbb{G}_1 \boldsymbol{\psi}_1$ where Z is the vacuum impedance and $\boldsymbol{\psi}_1$ the polarization field, which is zero in vacuum regions. Correspondingly, the current at ω_2 is given by

$$\mathbf{J}_2 = -i\omega_2 \alpha \frac{iZ}{k_1} \mathbb{P}_r (\mathbf{S}_1 + \mathbb{G}_1 \boldsymbol{\psi}_1) \quad (5)$$

where $\mathbf{S}_1 = \frac{k_1}{iZ} \mathbf{E}_{i,1}$ is defined for convenience. Note that the global phase factor in (5) is irrelevant for the objective in (4) and that we assume all Raman sources in \mathbb{P}_r are emitting in phase; this assumption trivially holds for a single Raman molecule. The total field at ω_2 can then be expressed in terms of the polarization field $\boldsymbol{\psi}_2(\mathbf{r}, \omega_2)$ via

$$\mathbf{E}_2 = \frac{iZ}{k_2} \mathbb{G}_2 (\mathbf{J}_2 + \boldsymbol{\psi}_2). \quad (6)$$

where again we neglect higher-order Raman effects such as down-conversion and work within the undepleted-pump approximation [17]. Following the same procedure introduced in recent works [10], one can write the optimization problem over Raman fields as a Quadratically Constrained Quadratic Program (QCQP) over the polarization fields $\boldsymbol{\psi}_1, \boldsymbol{\psi}_2$, with quadratic (energy-conservation) constraints derived by taking known inner products of operator constraints (see Supplementary Material [18]). The resulting QCQP takes the form

$$\begin{aligned} \max_{\boldsymbol{\psi}_1, \boldsymbol{\psi}_2} \quad & f(\boldsymbol{\psi}_1, \boldsymbol{\psi}_2) \\ \text{s.t.} \quad & \int_{\Omega_k} \mathbf{S}_i^\dagger \cdot \boldsymbol{\psi}_j d\mathbf{r} = \int_{\Omega_k} \boldsymbol{\psi}_i^\dagger (\chi_i^{-\dagger} - \mathbb{G}_i^\dagger) \cdot \boldsymbol{\psi}_j d\mathbf{r}, \quad (7) \\ & \frac{\text{Im} \chi_2}{|\chi_2|^2} \int_{\Omega} \boldsymbol{\psi}_2^\dagger \cdot \boldsymbol{\psi}_2 \leq \int_{\Omega} \mathbf{J}_2^\dagger \mathbb{G}_2^\dagger \cdot \mathbb{G}_2 \mathbf{J}_2 d\mathbf{r} \end{aligned}$$

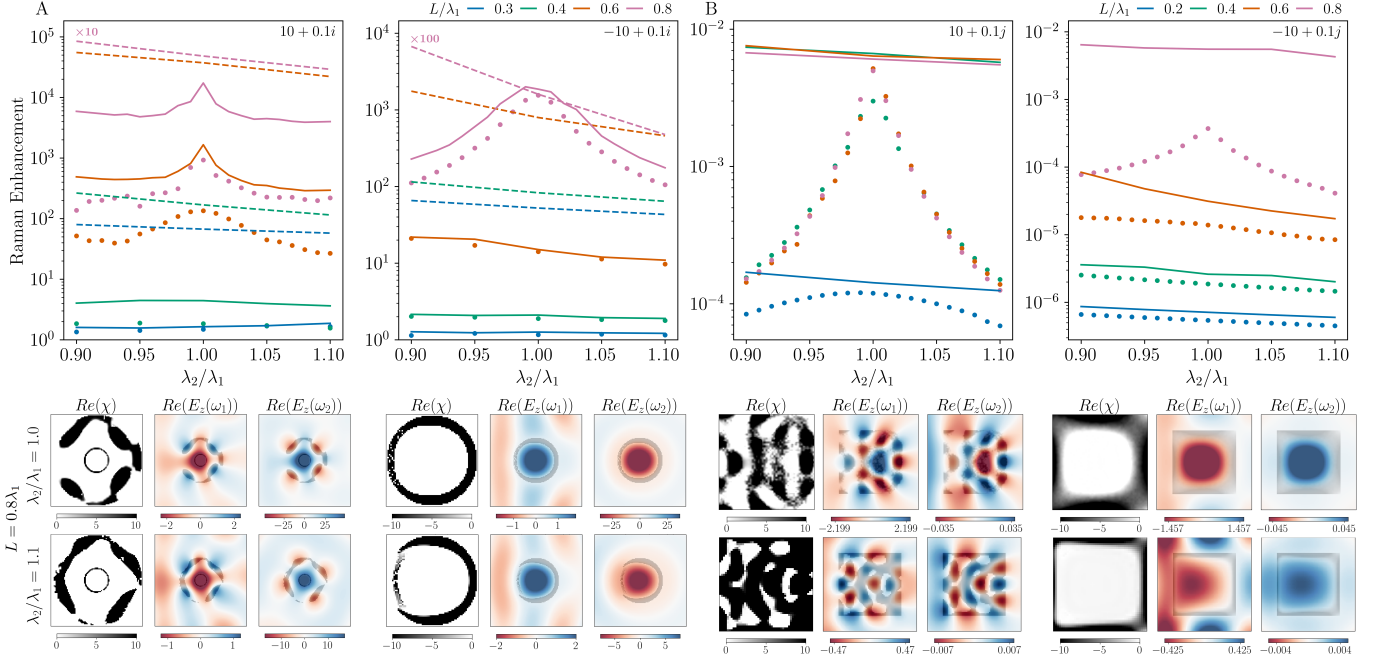


FIG. 2. Limits (lines) and associated inverse designs (dots) pertaining to the maximum achievable Raman enhancement from an incident planewave on either (A) a Raman molecule surrounded by a structured medium (an antenna) contained within a circular design region of inner diameter $d/\lambda_1 = 0.2$ and outer diameter L/λ_1 or (B) a Raman-active medium contained within a square of side-length L/λ_1 . The Raman enhancement is defined as the ratio of net scattered power f_{scat} in the presence and absence of the medium (A), or f_{scat} over the incident power (B). Both dielectric ($\chi_{1,2} = 10 + 0.1i$) and metallic ($\chi_{1,2} = -10 + 0.1i$) media are considered.

where $i, j \in \{1, 2\}$, χ_i is the bulk susceptibility of the linear medium at ω_i , and f is the quadratic objective function. Furthermore, $\mathbf{S}_2 = \mathbb{G}_2 \mathbf{J}_2$ may be interpreted as the Raman-induced field incident on the linear medium. The imposed constraints hold for all and any sub-regions $\Omega_k \subset \Omega$ of the total design region. As described in the SM [18], the last constraint, which follows from passivity, is required only for numerical reasons. The solution of the Lagrange dual to (7) for a given \mathbb{P}_r is a geometry-independent bound on the the primal objective. A full derivation of these constraints, including expanding all instances of \mathbf{J}_2 in terms of the optimization variables ψ_1, ψ_2 , is presented in the SM [18]. Detailed calculations of the corresponding Lagrange dual, gradients, and proof of the existence of a bound are also shown in the SM.

For the *Raman medium* case illustrated in Fig. 1(B), the structured medium itself is the Raman scatterer, so that $\alpha(\mathbf{r}) = \alpha^{\mathbb{P}}(\mathbf{r}) = \alpha^{\mathbb{P}_r}(\mathbf{r})$. Here, we relax \mathbf{J}_2 to an optimization degree of freedom and enforce inner products over (5) as additional constraints. Maintaining the same

definitions as above, the resulting QCQP takes the form

$$\begin{aligned}
 & \max_{\{\psi_1, \psi_2, \mathbf{J}_2\}} f(\psi_1, \psi_2, \mathbf{J}_2) \\
 & \text{s.t.} \quad \int_{\Omega_k} \mathbf{S}_i^\dagger \cdot \psi_j d\mathbf{r} = \int_{\Omega_k} \psi_i^\dagger (\chi_i^{-\dagger} - \mathbb{G}_i^\dagger) \cdot \psi_j d\mathbf{r}, \\
 & \quad \int_{\Omega_k} \mathbf{S}_i^\dagger \cdot \mathbf{J}_2 d\mathbf{r} = \int_{\Omega_j} \psi_i^\dagger (\chi_i^{-\dagger} - \mathbb{G}_i^\dagger) \cdot \mathbf{J}_2 d\mathbf{r}, \\
 & \quad \int_{\Omega_j} \mathbf{J}_2^\dagger \cdot \mathbf{J}_2 d\mathbf{r} = \left| \frac{\omega_2}{\omega_1 \chi_1} \right|^2 \int_{\Omega_j} \psi_1^\dagger \alpha^\dagger \cdot \alpha \psi_1 d\mathbf{r},
 \end{aligned} \tag{8}$$

Note that the last constraint is phase-agnostic and that by promoting \mathbf{J}_2 to an optimization degree of freedom, we allow variations in its phase profile. A bound on this problem is therefore also a bound on a medium containing a uniform distribution of fluctuating, spatially uncorrelated (out-of-phase) Raman scatterers [19]. Calculation of the Lagrange dual is presented in the SM [18].

Applications.— In what follows, we exploit the framework above to obtain upper bounds on the maximum allowed scattered power $f_{\text{scat}}(\psi_1, \psi_2) = -\frac{1}{2} \text{Re} \int_{\Omega} \mathbf{J}_2^* \cdot \mathbf{E}_2 d\mathbf{r} - \int_{\Omega} \psi_2^* \frac{\text{Im} \chi_2}{|\chi_2|^2} \frac{Z}{2k_2} \psi_2 d\mathbf{r}$ achievable in two canonical typical configurations. f_{scat} can be written purely in terms of coupled ψ_1, ψ_2 fields (see SM). To assess the importance of co-designing for both pump and

signal processes, we also compare results of bounding the full problem of (2) for a Raman molecule against those made possible via the linearized optimization problems (3) and (4).

Raman molecule: we first consider the maximum achievable scattered power f_{scat} that may arise from a TM (electric field out of plane) planewave of wavelength λ_1 incident on a Raman particle of polarizability $\alpha(\mathbf{r}) = \alpha\delta(\mathbf{r} - \mathbf{r}_0)$ at the center \mathbf{r}_0 of a circular design region of inner diameter $d/\lambda_1 = 0.2$ and outer diameter $L/\lambda_1 \in \{0.3, 0.4, 0.6, 0.8\}$. The Raman enhancement factor is defined as $f_{\text{scat}}(\psi_1, \psi_2)/f_{\text{scat}}(\mathbf{0})$, where $f_{\text{scat}}(\mathbf{0})$ represents the extracted power in the absence of the linear scatterer. The circular design region consists of either a dielectric ($\chi_1 = \chi_2 = 10 + 0.1i$) or metallic ($\chi_1 = \chi_2 = -10 + 0.1i$) medium. As shown in Fig. 2(A), bounds (solid lines) follow trends seen in topology-optimized designs (dots) over a broad range of signal wavelengths $\lambda_1/\lambda_2 \in [0.9, 1.1]$, peaking at the resonant condition $\lambda_2/\lambda_1 = 1$. As seen, the performance of dielectric structures is generally found to be within an order of magnitude of the bound for $L \leq 0.6\lambda_1$, becoming worse with increasing system size. Bounds on metals not only predict trends, anticipating the minimum design size needed to reach the resonant regime (the peak near $\lambda_2/\lambda_1 \sim 1$), but are also within factors of unity of inverse designs. Note that when adapted to bound extracted power, our performance metrics improve upon existing state-of-the-art [5] by more than four orders of magnitude (see SM [18]).

Field profiles reveal resonances exhibiting high field concentrations near the Raman molecule and large coupling to the incident planewave at λ_1 , illustrating the relative difficulty and importance of co-designing two resonances at different frequencies. To quantify the importance of structures designed for simultaneous operation at both wavelengths as dictated by the fully coupled non-linear problem of (2), Fig. 2(A) also shows limits (dashed lines) obtained by solving the “linearized”, independent problems of (4) and (3), as outlined in the SM [18]. In particular, the relaxation overestimates achievable signals by up to four orders of magnitude, failing to capture the design trade-offs and performance costs incurred by the need to simultaneously enhance both processes. This overestimation occurs even when $\lambda_1 = \lambda_2$ owing to the different design criteria necessary to achieve field focusing or scattering. Finally, Fig. 3 shows the scaling behavior of the maximum achievable scattered power f_{scat} with respect to system size L/λ_1 in the resonant case $\lambda_2 = \lambda_1$. For large enough systems, metals and dielectrics are found to converge to same maximum performance, suggesting that given sufficient structural freedom, the maximum Raman response is not limited by material choice. While dielectrics provably outperform metals in the subwavelength regime, this is expected to reverse for

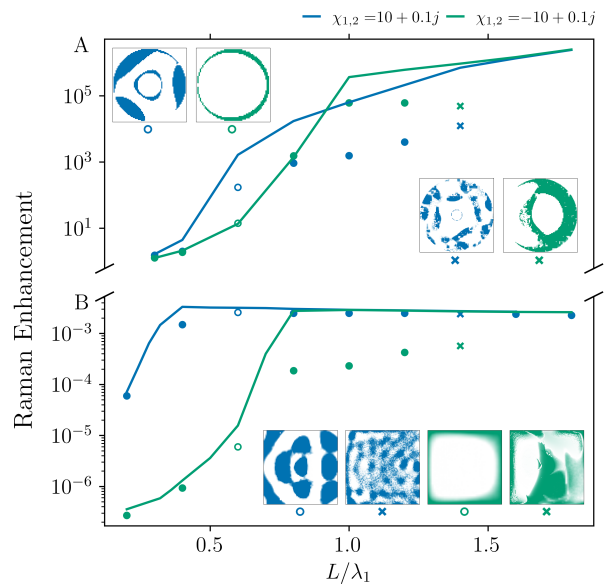


FIG. 3. Limits (lines) and associated inverse designs (dots) pertaining to maximum f_{scat} as a function of device size L/λ_1 for equivalent problem formulations as in Fig. 2 with $\lambda_1 \equiv \lambda_2$.

TE (in-plane electric) fields.

Raman medium: next, we consider the maximum achievable scattered power f_{scat} that may arise from a TM planewave of wavelength λ_1 incident on a Raman-active square design region of either dielectric ($\chi_1 = \chi_2 = 10 + 0.1i$) or metal ($\chi_1 = \chi_2 = -10 + 0.1i$) susceptibilities, Raman polarizability $\alpha = 0.01$, and of side length $L/\lambda_1 \in \{0.3, 0.4, 0.6, 0.8\}$, over a range of $\lambda_1/\lambda_2 \in [0.9, 1.1]$. The Raman enhancement factor is defined as the ratio of scattered power at ω_2 to incident power at ω_1 . As shown in Fig. 2(B), bounds come within an order of magnitude of achievable performance when no resonant peak is present. Limits pertaining to dielectric structures accurately predict performance of optimized devices when the Raman shift is negligible ($\lambda_1 \sim \lambda_2$), while failing to capture non-resonant behavior. Similar behavior is observed for metals, except that the performance gap grows with increasing system sizes to over an order of magnitude at the largest $L = 0.8\lambda$ sizes explored. As in the case of Raman particles, field profiles show metallic designs supporting resonances at both the pump and Raman wavelengths and demonstrate the non-reciprocity of the focusing and scattering problems. Unlike the previous case, structural information of the Raman scatterer is not known a priori so the bounds cannot be compared to their decoupled counterparts. Finally, as shown in Fig. 3, the scaling behavior of the bounds on resonant ($\lambda_1 = \lambda_2$) Raman enhancement with L/λ_1 come within factors of unity of achievable performance for dielectrics for all device sizes and within an order of magnitude for metals when the device is sufficiently small

($L/\lambda_1 \leq 0.3$) or large ($L/\lambda_1 \geq 0.6$). The shrinking gap between performance and bound for large device sizes is attributable to the saturation of the limits to a response not limited by material choice.

Concluding remarks.— While the typical approach of separately treating field-focusing and signal-extraction processes offers conceptual and computational simplifications, the presented comparisons of bounds that either incorporate or ignore structural coupling between the pump and Raman fields reveals the necessity of modelling the full non-linear problem. Such an analysis was made possible by generalizing a recent quadratic optimization method previously restricted to linear electromagnetic problems [10]. By taking into account full structural coupling in the objective, these results not only greatly improve on existing bounds [5] but also pave the way for studying designable Raman-active structures.

Acknowledgements.— We would like to thank Jewel Mohajan and Steven G. Johnson for useful discussions.

Funding.— We acknowledge the support by a Princeton SEAS Innovation Grant and by the Cornell Center for Materials Research (MRSEC). SM also acknowledges financial support from IVADO (Institut de valorisation des données, Québec). The simulations presented in this article were performed on computational resources managed and supported by Princeton Research Computing, a consortium of groups including the Princeton Institute for Computational Science and Engineering (PICSciE) and the Office of Information Technology’s High Performance Computing Center and Visualization Laboratory at Princeton University.

* alessioamaolo@princeton.edu

- [1] E. C. Le Ru and P. G. Etchegoin, *Principles of surface-enhanced Raman spectroscopy: and related plasmonic effects*, 1st ed. (Elsevier, Amsterdam; Boston, 2009).
- [2] H. Rong, R. Jones, A. Liu, O. Cohen, D. Hak, A. Fang, and M. Paniccia, A continuous-wave raman silicon laser, *Nature* **433**, 725–728 (2005).
- [3] X. X. Han, R. S. Rodriguez, C. L. Haynes, Y. Ozaki, and B. Zhao, Surface-enhanced raman spectroscopy, *Nature Reviews Methods Primers* **1**, 1–17 (2022).
- [4] R. E. Christiansen, J. Michon, M. Benzaouia, O. Sigmund, and S. G. Johnson, Inverse design of nanoparticles for enhanced raman scattering, *Optics Express* **28**, 4444–4462 (2020).
- [5] J. Michon, M. Benzaouia, W. Yao, O. D. Miller, and S. G. Johnson, Limits to surface-enhanced raman scattering near arbitrary-shape scatterers, *Optics Express* **27**, 35189–35202 (2019).
- [6] L. Long, W. Ju, H.-Y. Yang, and Z. Li, Dimensional design for surface-enhanced raman spectroscopy, *ACS Materials Au* **2**, 552–575 (2022).
- [7] J. Lu, D. Zhang, Q. Chen, Z. Shang, J. Huang, and P. Liang, Nanoparticles/parabolic nanobowl hybrid structure as a surface-enhanced raman scattering substrate: Insights using the FDTD method, *The Journal of Physical Chemistry C* **126**, 14211–14218 (2022).
- [8] G. Angeris, J. Vučković, and S. P. Boyd, Computational bounds for photonic design, *ACS Photonics* **6**, 1232–1239 (2019).
- [9] S. Molesky, P. Chao, J. Mohajan, W. Reinhart, H. Chi, and A. W. Rodriguez, \mathbb{T} -operator limits on optical communication: Metaoptics, computation, and input-output transformations, *Physical Review Research* **4**, 013020 (2022).
- [10] P. Chao, B. Strekha, R. Kuate Defo, S. Molesky, and A. W. Rodriguez, Physical limits in electromagnetism, *Nature Reviews Physics* **4**, 543–559 (2022).
- [11] Z. Kuang and O. D. Miller, Computational bounds to light–matter interactions via local conservation laws, *Physical Review Letters* **125**, 263607 (2020).
- [12] M. Gustafsson, K. Schab, L. Jelinek, and M. Capek, Upper bounds on absorption and scattering, *New Journal of Physics* **22**, 073013 (2020).
- [13] J. Mohajan, P. Chao, W. Jin, S. Molesky, and A. W. Rodriguez, Fundamental limits on radiative $\chi^{(2)}$ second harmonic generation, *Optics Express* **31**, 44212–44223 (2023).
- [14] H. Rong, S. Xu, Y.-H. Kuo, V. Sih, O. Cohen, O. Raday, and M. Paniccia, Low-threshold continuous-wave raman silicon laser, *Nature Photonics* **1**, 232–237 (2007).
- [15] T. Ideguchi, S. Holzner, B. Bernhardt, G. Guelachvili, N. Picqué, and T. W. Hänsch, Coherent raman spectro-imaging with laser frequency combs, *Nature* **502**, 355–358 (2013).
- [16] R. Claps, D. Dimitropoulos, V. Raghunathan, Y. Han, and B. Jalali, Observation of stimulated raman amplification in silicon waveguides, *Optics Express* **11**, 1731–1739 (2003).
- [17] R. W. Boyd, *Nonlinear Optics* (Academic Press, 2003).
- [18] See Supplemental Material for derivation and solution of the Lagrange dual problem, expansion of objectives and constraints in terms of optimization fields, a description of the method for bounding the structurally decoupled Raman enhancement problem, and comparison of these bounds with prior work.
- [19] W. Yao, F. Verdugo, H. O. Everitt, R. E. Christiansen, and S. G. Johnson, Designing structures that maximize spatially averaged surface-enhanced raman spectra, *Optics Express* **31**, 4964–4977 (2023).

Supplemental Material for “Physical Limits on Raman Scattering: The Critical Role of Pump and Signal Co-design”

Alessio Amaolo, Pengning Chao, Thomas J. Maldonado, Sean Molesky, Alejandro W. Rodriguez
(Dated: March 7, 2024)

DERIVATION OF RAMAN QCQP

We write Maxwell’s equations for Raman scattering as:

$$\nabla \times \nabla \times \mathbf{E}_1 - k_1^2 \mathbb{V}(\mathbf{r}, \omega_1) \mathbf{E}_1 = i\omega_1 \mathbf{J}_{\text{vac}} \quad (\text{S1a})$$

$$\nabla \times \nabla \times \mathbf{E}_2 - k_2^2 \mathbb{V}(\mathbf{r}, \omega_2) \mathbf{E}_2 = \omega_2^2 \alpha(r) \mathbf{E}_1 = i\omega_2 \mathbf{J}_2 \quad (\text{S1b})$$

where \mathbf{E}_1 is field sourced by some initial current (for example a dipole), \mathbf{E}_2 is the Raman scattered field, $k_i = \omega_i/c$, $\alpha(\mathbf{r})$ is the Raman polarizability tensor, $\mathbb{V}(\mathbf{r}, \omega_j)$ is the permittivity profile at ω_j , $\mathbf{J}_2 \equiv -i\omega_2 \alpha \mathbf{E}_1$, and $\epsilon_0 = 1$. We consider nonmagnetic materials and set $\mu = 1$. To simplify algebra and complicated integrals, these sections will make use of bra-ket notation to mean conjugated inner products.

Design material near a known Raman scatterer. The simplest case is a linear design material near a known Raman scatterer. We write $\alpha(r) \rightarrow \alpha \mathbb{P}_r$ where α is a constant polarizability tensor and \mathbb{P}_r is an operator that projects onto the Raman material. We define \mathbb{G}_i as the operator form of the Green’s function of the vacuum Maxwell operator \mathbb{M}_i such that $\mathbb{M}_i \mathbb{G}_i = k_i^2$. By splitting \mathbb{G}_i into the design region and Raman scattering regions (which we assume to be disjoint), we can write

$$\mathbb{G}_i = \begin{bmatrix} \mathbb{G}_{i,dd} & \mathbb{G}_{i,dr} \\ \mathbb{G}_{i,rd} & \mathbb{G}_{i,rr} \end{bmatrix}, \quad \mathbb{P}_r = [0 \ \mathbb{I}_{r,r}], \quad \mathbb{P} = [\mathbb{I}_{d,d} \ 0], \quad (\text{S2})$$

where we have defined \mathbb{P} as an operator that projects a full vector (including the design and Raman region) into the design region. In bra-ket notation, we keep track of the scattering of the fields:

$$|E_{i,1}\rangle = \frac{iZ}{k_1} \mathbb{G}_1 |J_{\text{vac}}\rangle \equiv \frac{iZ}{k_1} |S_1\rangle \quad \text{Known incident field at } \omega_1 \quad (\text{S3a})$$

$$|E_{s,1}\rangle = \frac{iZ}{k_1} \mathbb{G}_{1,dd} |\psi_1\rangle \quad \text{Scattered field in device at } \omega_1 \quad (\text{S3b})$$

$$|J_2\rangle = -i\omega_2 \alpha \frac{iZ}{k_1} (\mathbb{P}_r |S\rangle + \mathbb{G}_{1,rd} |\psi_1\rangle) \quad \text{Raman source current at } \omega_2 \quad (\text{S3c})$$

$$|E_{i,2}\rangle = \frac{iZ}{k_2} \mathbb{G}_{2,dr} |J_2\rangle \equiv \frac{iZ}{k_2} |S_2\rangle \quad \text{Raman field produced by Raman material at } \omega_2 \quad (\text{S3d})$$

$$|E_{s,2}\rangle = \frac{iZ}{k_2} \mathbb{G}_{2,dd} |\psi_2\rangle \quad \text{Raman field scattered by linear material at } \omega_2 \quad (\text{S3e})$$

where we’ve defined $|\psi_1\rangle \equiv \mathbb{T}_1 \mathbb{G}_1 |J_{\text{vac}}\rangle$ for the $\mathbb{T}_i = (\chi_i^{-1} - \mathbb{G}_{i,dd})^{-1}$ operator defined in [4], and $|\psi_2\rangle \equiv \mathbb{T}_2 \mathbb{G}_2 |J_2\rangle$ is the polarization current in the linear material induced by $|E_{i,2}\rangle$. We neglect the effects of $|E_{s,2}\rangle$ further interacting with the Raman scatterer. Our optimization vectors will be the polarization currents $|\psi_1\rangle, |\psi_2\rangle$ in the design region.

Let χ_1, χ_2 be the susceptibilities of the linear material at ω_1, ω_2 respectively. The objectives treated in the text are

$$f_{\text{ext}} = \underbrace{-\frac{1}{2} \text{Re} \langle J_2 | E_2 \rangle}_{\text{extracted power}}, \quad f_{\text{scat}} = f_{\text{ext}} - \underbrace{\langle \psi_2 | \frac{\text{Im} \chi_2}{|\chi_2|^2} \frac{Z}{2k_2} |\psi_2 \rangle}_{\text{absorbed power}}. \quad (\text{S4})$$

Expanding in terms of the optimization variables,

$$\begin{aligned} f_{\text{ext}} = & \frac{1}{2} \text{Im} \frac{\omega_2^\dagger}{\omega_1^\dagger \omega_2} \left(\langle \psi_1 | \mathbb{G}_{1,rd}^\dagger \alpha^\dagger \mathbb{G}_{2,rd} |\psi_2\rangle + \langle S_1 | \mathbb{P}_r^\dagger \alpha^\dagger \mathbb{G}_{2,rd} |\psi_2\rangle \right) \\ & + \frac{1}{2} \text{Im} \frac{\omega_2^\dagger}{|\omega_1|} \left(\langle \psi_1 | \mathbb{G}_{1,rd}^\dagger \alpha^\dagger \mathbb{G}_{2,rr} \alpha \mathbb{G}_{1,rd} |\psi_1\rangle + \langle S_1 | \mathbb{P}_r^\dagger \alpha^\dagger \mathbb{G}_{2,rr} \alpha \mathbb{G}_{1,rd} |\psi_1\rangle \right. \\ & \left. + \langle \psi_1 | \mathbb{G}_{1,rd}^\dagger \alpha^\dagger \mathbb{G}_{2,rr} \alpha \mathbb{P}_r |S_1\rangle + \langle S_1 | \mathbb{P}_r^\dagger \alpha^\dagger \mathbb{G}_{2,rr} \alpha \mathbb{P}_r |S_1\rangle \right). \end{aligned} \quad (\text{S5})$$

The constraints are derived from identity relations on the \mathbb{T} operators: $\mathbb{P}_j = \mathbb{T}_i^\dagger \mathbb{U}_i \mathbb{P}_j$ for operators \mathbb{P}_j that project onto any sub-region j and $\mathbb{U}_i \equiv (\chi_i^{-\dagger} - \mathbb{G}_{i,dd}^\dagger)$. Inner products with combinations of $|S_1\rangle$ and $|S_2\rangle$ give

$$\langle S_1 | p^\dagger \mathbb{P}_j | \psi_1 \rangle = \langle \psi_1 | \mathbb{U}_1 \mathbb{P}_j | \psi_1 \rangle, \quad (\text{S6a})$$

$$\frac{\omega_2^\dagger}{\omega_1^\dagger} \left(\langle \psi_1 | \mathbb{G}_{1,rd}^\dagger \alpha^\dagger \mathbb{G}_{2,dr}^\dagger \mathbb{P}_j | \psi_2 \rangle + \langle S_1 | \mathbb{P}_r^\dagger \alpha^\dagger \mathbb{G}_{2,dr}^\dagger \mathbb{P}_j | \psi_2 \rangle \right) = \langle \psi_2 | \mathbb{U}_2 \mathbb{P}_j | \psi_2 \rangle, \quad (\text{S6b})$$

$$\langle S_1 | p^\dagger \mathbb{P}_j | \psi_2 \rangle = \langle \psi_1 | \mathbb{U}_1 \mathbb{P}_j | \psi_2 \rangle, \quad (\text{S6c})$$

$$\frac{\omega_2^\dagger}{\omega_1^\dagger} \left(\langle \psi_1 | \mathbb{G}_{1,rd}^\dagger \alpha^\dagger \mathbb{G}_{2,dr}^\dagger \mathbb{P}_j | \psi_1 \rangle + \langle S_1 | \mathbb{P}_r^\dagger \alpha^\dagger \mathbb{G}_{2,dr}^\dagger \mathbb{P}_j | \psi_1 \rangle \right) = \langle \psi_2 | \mathbb{U}_2 \mathbb{P}_j | \psi_1 \rangle. \quad (\text{S6d})$$

The dual problem is solved using an interior point method, requiring an initial feasible point. To find it, we enforce the passivity constraint $\frac{\text{Im } \chi}{|\chi|^2} \langle \psi_2 | \psi_2 \rangle \leq \text{Asym} \langle \psi_2 | \mathbb{G}_{2,dr} | J_2 \rangle$, which is trivially satisfied if (S6b) is satisfied. Noting that

$$\text{Asym} \langle \psi_2 | \mathbb{G}_{2,dr} | J_2 \rangle \leq \sqrt{\langle \psi_2 | \psi_2 \rangle} \sqrt{\langle J_2 | \mathbb{G}_{2,dr}^\dagger \mathbb{G}_{2,dr} | J_2 \rangle}$$

and expanding in terms of optimization variables, the convex inequality constraint becomes

$$- \left(\frac{\text{Im } \chi}{|\chi|^2} \right)^2 \langle \psi_2 | \psi_2 \rangle + \frac{|\omega_2|^2}{|\omega_1|^2} \left(\langle S_1 | \mathbb{P}_r^\dagger + \langle \psi_1 | \mathbb{G}_{1,rd}^\dagger \right) \alpha^\dagger \mathbb{G}_{2,dr}^\dagger \mathbb{G}_{2,dr} \alpha \left(\mathbb{P}_r | S_1 \rangle + \mathbb{G}_{1,rd} | \psi_1 \rangle \right) \geq 0. \quad (\text{S7})$$

To find an initial feasible point, where the matrix Z^{TT} (see below) is positive-definite, we note that the positive semi-definiteness of $\text{Im } \mathbb{G}_{i,dd}$ and the assumption that $\text{Im } \chi > 0$ guarantees that for some small Lagrange multiplier corresponding to Eq. S7, there exists some sufficiently large Lagrange multiplier corresponding to Eq. S6a that makes Z^{TT} positive definite.

Raman Active Design Material. We take $\alpha \mathbb{P}_r \rightarrow \alpha \mathbb{P}$ such that the Raman scatterer is only present where material is present. To ensure bounds are structure independent, we relax $|J_2\rangle$ to an optimization degree of freedom. The scattered power objective is:

$$f_{\text{scat}} = \frac{Z}{2k_2} \left[\text{Im} \left(\langle J_2 | \mathbb{G}_0^{(2)} | J_2 \rangle + \langle J_2 | \mathbb{G}_0^{(2)} | \psi_2 \rangle \right) - \langle \psi_2 | \frac{\text{Im } \chi_2}{|\chi_2|^2} | \psi_2 \rangle \right]. \quad (\text{S8})$$

The constraints are derived from the same identities as above. Inner products with incident fields and $|J_2\rangle$ give

$$\langle S_1 | \mathbb{P}_j | \psi_1 \rangle = \langle \psi_1 | \mathbb{U}_1 \mathbb{P}_j | \psi_1 \rangle, \quad (\text{S9a})$$

$$\langle J_2 | \mathbb{G}_2^\dagger \mathbb{P}_j | \psi_2 \rangle = \langle \psi_2 | \mathbb{U}_2 \mathbb{P}_j | \psi_2 \rangle, \quad (\text{S9b})$$

$$\langle S_1 | \mathbb{P}_j | \psi_2 \rangle = \langle \psi_1 | \mathbb{U}_1 \mathbb{P}_j | \psi_2 \rangle, \quad (\text{S9c})$$

$$\langle S_1 | \mathbb{P}_j | J_2 \rangle = \langle \psi_1 | \mathbb{U}_1 \mathbb{P}_j | J_2 \rangle, \quad (\text{S9d})$$

$$\langle J_2 | \mathbb{G}_2^\dagger \mathbb{P}_j | \psi_1 \rangle = \langle \psi_2 | \mathbb{U}_2 \mathbb{P}_j | \psi_1 \rangle. \quad (\text{S9e})$$

By taking an inner product of $|J_2\rangle$ with itself, we find the additional constraint

$$\langle J_2 | \mathbb{P}_j | J_2 \rangle = \left| \frac{\omega_2}{\omega_1 \chi_1} \right|^2 \langle \psi_1 | \alpha^\dagger \mathbb{P}_j \alpha | \psi_1 \rangle. \quad (\text{S10})$$

Calculation of Lagrange dual. Writing the Lagrangian

$$\mathcal{L}(\psi, S) = [\langle \psi_{\text{opt}} | \langle S |] \begin{bmatrix} -Z^{TT}(\lambda) & Z^{TS}(\lambda) \\ Z^{ST}(\lambda) & Z^{SS}(\lambda) \end{bmatrix} \begin{bmatrix} |\psi_{\text{opt}} \rangle \\ |S \rangle \end{bmatrix}, \quad (\text{S11})$$

where $\psi_{\text{opt}} = [\psi_1, \psi_2]^T$ in the Raman-active particles case and $\psi_{\text{opt}} = [\psi_1, \psi_2, J_2]^T$ in the Raman-active design material case. The Lagrange dual and its derivatives can be written, in terms of $|\psi^*\rangle = Z^{TT-1} Z^{TS} |S\rangle$ and for positive definite Z^{TT} ,

$$\begin{aligned} \mathcal{G}(\lambda) &= \langle S | Z^{ST} Z^{TT-1} Z^{TS} + Z^{SS} | S \rangle, \\ \frac{\partial \mathcal{G}}{\partial \lambda} &= 2 \text{Re} \left(\langle \psi^* | \frac{\partial Z^{TS}}{\partial \lambda} | S \rangle \right) - \langle \psi^* | \frac{\partial Z^{TT}}{\partial \lambda} | \psi^* \rangle + \langle S | \frac{\partial Z^{SS}}{\partial \lambda} | S \rangle. \end{aligned} \quad (\text{S12})$$

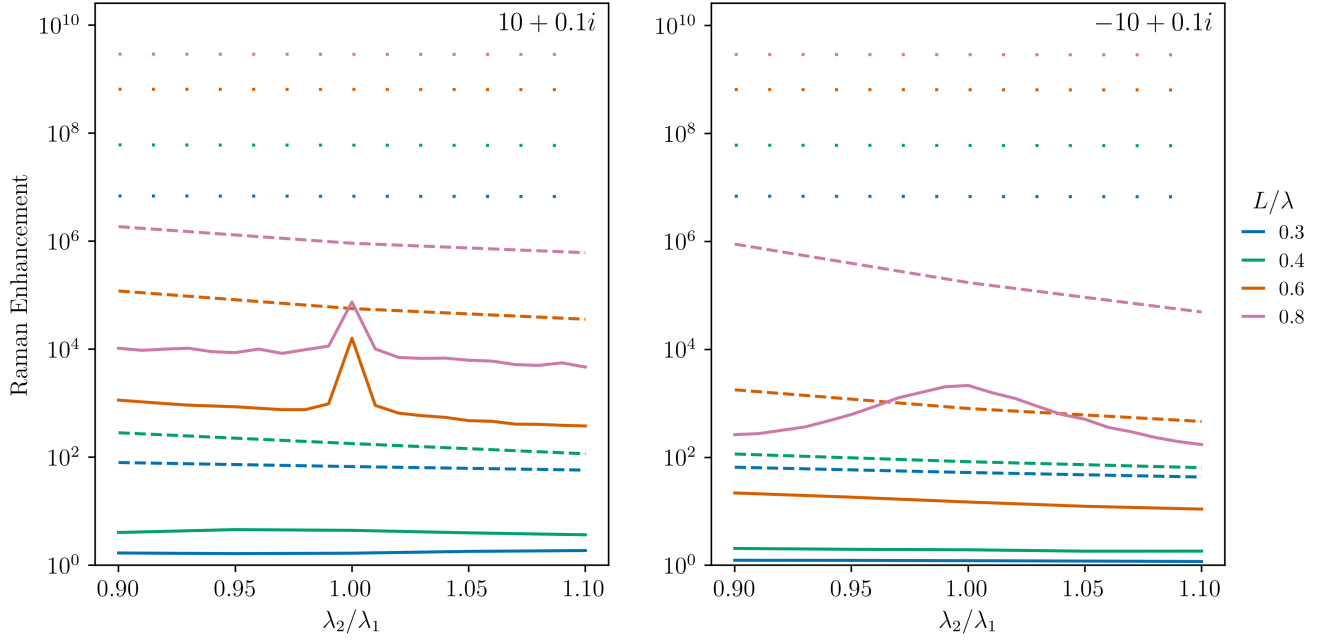


FIG. S1: Bounds on the Raman particles problem as described in the main text, replacing $f_{\text{scat}} \rightarrow f_{\text{ext}}$ for fair comparison to existing work. Limits are computed with our coupled method (solid), our decoupled method (dashed) and methods in [3] (dotted). These results make clear the significant improvement in these bounds achieved by the methods in this article.

BOUNDING DECOUPLED RAMAN-ENHANCEMENT PROBLEM

Focusing. The field-focusing optimization problem takes the form

$$\begin{aligned} \max_{|\psi_1\rangle} \quad & \frac{Z^2}{|k_1|^2} \left[\langle S_1 | \mathbb{P}_r^\dagger \alpha^\dagger \alpha \mathbb{P}_r | S_1 \rangle + 2 \operatorname{Re} \langle \psi_1 | \mathbb{G}_{1,rd}^\dagger \alpha^\dagger \alpha \mathbb{P}_r | S_1 \rangle + \langle \psi_1 | \mathbb{G}_{1,rd}^\dagger \alpha^\dagger \alpha \mathbb{G}_{1,rd} | \psi_1 \rangle \right] \\ \text{s.t.} \quad & \langle S_1 | \mathbb{P}_j | \psi_1 \rangle - \langle \psi_1 | \mathbb{U}_1 \mathbb{P}_j | \psi_1 \rangle = 0 \end{aligned} \quad (\text{S13})$$

A bound b_{focus} can be computed via the Lagrange dual as above where $\psi_{\text{opt}} = \psi_1$. The bound on the amplitude $\langle J_2 | J_2 \rangle$ of the Raman-active dipole is therefore $M_f \equiv \omega_2^2 b_{\text{focus}}$.

Scattered power. The scattering optimization problem takes the form

$$\begin{aligned} \max_{|\psi_2\rangle} \quad & \frac{Z}{2k_2} \operatorname{Im} \langle S_2 | \psi_2 \rangle - \frac{Z}{2k_2} \langle \psi_2 | \frac{\operatorname{Im} \chi_2}{|\chi_2|^2} | \psi_2 \rangle \\ \text{s.t.} \quad & \langle S_2 | \mathbb{P}_j | \psi_2 \rangle - \langle \psi_2 | \mathbb{U}_2 \mathbb{P}_j | \psi_2 \rangle = 0 \end{aligned} \quad (\text{S14})$$

where in the Raman molecule case, the incident field from the Raman scatterer $|S_2\rangle$ is treated as a unit dipole field. A bound M_l can be computed using the methods above where $|\psi_{\text{opt}}\rangle = |\psi_2\rangle$.

The final decoupled bound on the Raman enhancement problem is $M_f M_l$.

COMPARISON TO EXISTING BOUNDS

For a fair comparison of our bounds with existing methods, we calculate analogous bounds on f_{ext} for the Raman particles problem seen in the main text with the methods in [3]. Although these bounds were found to be tight in specific cases, our method exhibited many orders of magnitude improvement for the case studied in this paper. A direct comparison is shown in Figure S1.

COMPUTATIONAL DETAILS

Inverse design in this work was performed by linearly interpolating between vacuum and the design material χ_d via $\chi = \chi_d + (1 - \chi_d)\rho$ for $\rho \in [0, 1]$. Optimization over the interpolation variable ρ was done by solving the Maxwell problem using a custom Finite-Difference Frequency-Domain (FDFD) solver written in Jax [2], calculating derivatives with Jax built-in gradient capabilities, and performing projected gradient ascent to maximize the objective using Jaxopt [1].

-
- [1] Mathieu Blondel, Quentin Berthet, Marco Cuturi, Roy Frostig, Stephan Hoyer, Felipe Llinares-López, Fabian Pedregosa, and Jean-Philippe Vert. Efficient and modular implicit differentiation. *arXiv preprint arXiv:2105.15183*, 2021.
 - [2] James Bradbury, Roy Frostig, Peter Hawkins, Matthew James Johnson, Chris Leary, Dougal Maclaurin, George Necula, Adam Paszke, Jake VanderPlas, Skye Wanderman-Milne, and Qiao Zhang. JAX: composable transformations of Python+NumPy programs, 2018.
 - [3] Jérôme Michon, Mohammed Benzaouia, Wenjie Yao, Owen D. Miller, and Steven G. Johnson. Limits to surface-enhanced raman scattering near arbitrary-shape scatterers. *Optics Express*, 27(24):35189–35202, November 2019.
 - [4] Sean Molesky, Pengning Chao, Weiliang Jin, and Alejandro W. Rodriguez. Global \mathbb{T} operator bounds on electromagnetic scattering: Upper bounds on far-field cross sections. *Physical Review Research*, 2(3):033172, July 2020.